文章编号：1001-9014(XXXX)XX-0001-06

DOI:10.11972/j.issn.1001-9014.XXXX.XX.001

Modeling the electronic band-structure of strained long-wavelength Type-II superlattices using the scattering matrix method

Abbas Haddadi, Gail Brown, Manijeh Razeghi*

(Center for Quantum Devices, Department of Electrical Engineering and Computer Science, Northwestern University, Evanston, Illinois 60208, USA)

Abstract: This study introduces a comprehensive theoretical framework for accurately calculating the electronic band-structure of strained long-wavelength InAs/GaSb type-II superlattices. Utilizing an eight-band $k \cdot p$ Hamiltonian in conjunction with a scattering matrix method, the model effectively incorporates quantum confinement, strain effects, and interface states. This robust and numerically stable approach achieves exceptional agreement with experimental data, offering a reliable tool for analyzing and engineering the band structure of complex multilayer systems.

Key words: Type-II superlattices, Long-wavelength infrared (LWIR), Scattering matrix method, Electronic band-structure modeling, InAs/GaSb heterostructures, Infrared photodetectors, and Bandgap engineering

Introduction

Type-II InAs/GaSb superlattices (T2SLs), formed by alternating InAs and GaSb layers over multiple periods, were first proposed by Sai-Halasz, Tsu, and Esaki in 1977 [1]. These structures are characterized by a broken-gap alignment where the valence band maximum of GaSb lies above the conduction band minimum of InAs,

Received date: 2024-12-09, **revised date**: 2024-12-24　　**收稿日期**:2024-12-09,**修回日期**:2024-12-24

Biography: **Abbas Haddadi** received his Ph. D. in Electrical Engineering and Computer Science from Northwestern University, Evanston, IL, in 2015. He is currently a Display Architect at Apple, Inc., a role he has held since May 2022. Previously, He served as a Senior Research Scientist at KLA (2018 - 2022), where he worked on next-generation high-performance UV/Visible/Infrared image sensors and imaging systems. Prior to that, he was the Technical Director at Nour, LLC (2016 - 2018), contributing to the development of innovative infrared camera technologies. His research interests span compound semiconductor materials, epitaxial crystal growth, novel optoelectronic devices, high-speed optoelectronics and advanced imaging systems.

Gail J. Brown received the Ph. D. degree from the University of Dayton, Dayton, OH, USA, in 1994. She was a Principal Physicist with the Nanoelectronics Materials Branch, Materials and Manufacturing Directorate, Air Force Research Laboratory, where she worked from 1980 to 2017. She led a team of researchers involved in advanced electronic material research, such as multiferroic materials for microwave electronics, and semiconductor superlattices for infrared sensing. She is currently an Adjunct Professor with Northwestern University.

* **Corresponding author**: **Manijeh Razeghi** received the Doctorate d'état ES Sciences Physiques from the Université de Paris, France, in 1980.

Manijeh Razeghi was the Head of the Exploratory Materials Laboratory at Thomson-CSF (France) during the 80's where she developed and implemented modern metalorganic chemical vapor deposition (MOCVD) vapor phase epitaxy (VPE), molecular beam epitaxy (MBE), GasMBE, and MOMBE for entire compositional ranges of III-V compound semiconductors from deep UV to THZ. Developing these tools was fundamental in enabling her to achieve high purity semiconductor crystals with a consistency and reliability that was often unmatched, thereby leading to new physics phenomena in InP, GaAs, GaSb, and AlN based semiconductors and quantum structures. She realized the first InP Quantum wells and Superlattices and demonstrated the marvels of quantum mechanics in the low dimensional world.

She joined Northwestern University, Evanston, IL, as a Walter P. Murphy Professor and Director of the Center for Quantum Devices in Fall 1991, where she created the undergraduate and graduate program in solid-state engineering.

She has authored or co-authored more than 1000 papers, more than 35 book chapters, and 20 books, including the textbooks Technology of Quantum Devices (Springer Science Business Media, Inc., New York, NY U. S. A. 2010) and Fundamentals of Solid State Engineering, 4th Edition (Springer Science Business Media, Inc., New York, NY U. S. A. 2018). Two of her books, MOCVD Challenge Vol. 1 (IOP Publishing Ltd., Bristol, U. K., 1989) and MOCVD Challenge Vol. 2 (IOP Publishing Ltd., Bristol, U. K., 1995), discuss some of her pioneering work in InP-GaInAsP and GaAs-GaInAsP based systems. The MOCVD Challenge, 2nd Edition (Taylor & Francis/CRC Press, 2010) represents the combined updated version of Volumes 1 and 2. She holds many U. S. patents and has given more than 1000 invited and plenary talks. Her current research interest is in nanoscale optoelectronic quantum devices. From deep UV to Thz.

Dr. Razeghi is a Fellow of MRS, IOP, IEEE, APS, SPIE, OSA, Fellow and Life Member of Society of Women Engineers (SWE), and Fellow of the International Engineering Consortium (IEC). She received the IBM Europe Science and Technology Prize in 1987, the Achievement Award from the SWE in 1995, the R. F. Bun shah Award in 2004, IBM Faculty Award 2013, the Jan Czochralski Gold Medal in 2016, the 2018 Benjamin Franklin Medal in Electrical Engineering, LSA 10th Anniversary Outstanding Contribution Award, and many best paper awards. She is an elected life-Fellow of SWE, IEEE, and MRS. She is honored as a member of Academy of Europe 2021. E-mail: razeghi@northwestern.edu

resulting in the spatial separation of electrons in InAs and holes in GaSb. The tunable band-structure of T2SLs is one of their most significant advantages, as the energy gap can be engineered by varying the layer thicknesses and interface compositions. This tunability makes T2SLs a promising candidate for a wide range of applications, including photodetectors [2, 3] and lasers [4]. In particular, their narrow bandgap makes them especially well-suited for the development of long wavelength infrared (LWIR) photodetectors [3, 5-7].

Traditionally, methods such as the Empirical Tight Binding Method (ETBM) have been used to calculate electronic band structures in these systems [8]. However, ETBM heavily relies on material-specific fitting parameters, limiting its accuracy for narrow bandgaps relevant to LWIR applications. An alternative approach based on the $k\cdot p$ model and envelope function approximation offers improved accuracy by incorporating interface effects and strain.

In this work, we adopt an eight-band $k\cdot p$ model to construct the bulk states in individual material layers and match the wavefunctions at interfaces using the boundary conditions from Burt's envelope function theory [9]. This approach accounts for the impact of lattice-mismatch strain on the electronic band-structure of InAs/GaSb superlattices designed for LWIR photodetectors (around the Γ-point). To solve the eigenvalue problem, we employ the scattering-matrix method, which provides greater numerical stability than traditional transfer-matrix approaches, particularly for thicker structures and large basis sets (such as LWIR T2SLs). This method relies on fewer empirical parameters, incorporates strain and interface effects, and reduces computational complexity by handling smaller matrices. At the end, we compare the obtained results from the model with experimental results to confirm the predictions of this method.

1 Method

In this work, we consider a structure consisting of InAs/GaSb quantum wells grown along the [001] direction on a GaSb substrate (z-direction). While the study of bulk materials using the $k\cdot p$ model does not pose significant challenges, this is not the case for heterostructures like superlattices. The behavior of the envelope function at the interfaces between different semiconductors remains uncertain. However, Burt demonstrated that a Hamiltonian similar to the one proposed by Kane can be effectively applied to the bulk regions of a superlattice, provided the quadratic valence band terms are properly symmetrized [9]. This approach was later extended to an eight-band Hamiltonian by Foreman [10]. This eight-band $k\cdot p$ model is employed for zinc-blende crystals to describe the conduction and valence band structures near the Γ-point, with spin-orbit coupling and strain effects included. In this model, the contributions of higher bands are neglected, and spin-orbit coupling is treated as a perturbation [11]. Using the following basis functions $|S\uparrow\rangle, |X\uparrow\rangle, |Y\uparrow\rangle, |Z\uparrow\rangle, |S\downarrow\rangle, |X\downarrow\rangle, |Y\downarrow\rangle,$ and $|Z\downarrow\rangle$ [10], the 8×8 $k\cdot p$ Burt's Hamiltonian can be expressed as:

$$H=\begin{bmatrix}H_4 & 0\\ 0 & H_4\end{bmatrix}+H_{SO}+H_\varepsilon \tag{1}$$

where H_4 represents the k-dependent 4×4 block, H_{SO} accounts for spin-orbit coupling effects, and H_ε incorporates the strain-induced modifications in the electronic structure.

The H_4 block is defined as:

$$H_4=\begin{bmatrix}H_{cc} & H_{cv}\\ H_{vc} & H_{vv}\end{bmatrix}. \tag{2}$$

where the conduction band term is $H_{cc}=E_c(z)+kA_c(z)k$, with A_c representing contributions from remote bands [10]. The parameter A_c is given by:

$$A_c=\frac{\hbar^2}{2m_c}-\frac{P^2}{3E_g}-\frac{P^2}{3\left(E_g+\Delta\right)} \tag{3}$$

where m_c is the conduction band effective mass, P is the interband momentum matrix element defined as $P=(\hbar/im)\langle S|p_x|X\rangle$, E_g is the bandgap, Δ represents the spin-orbit splitting energy, and m is the free-electron mass.

The coupling between the conduction and valence bands is expressed as $H_{cv}=H_{cv}^{\dagger}=\left[iPk_x\ iPk_y\ iPk_z\right]$, where Kane's B-parameter is neglected. The valence band block H_{vv} is a 3×3 matrix that describes the interactions among heavy-hole, light-hole, and split-off states with typical diagonal and off. Its diagonal components are given by:

$$\begin{aligned}H_{XX}&=E_v-\frac{\Delta}{3}+L'K_x^2+M\left(k_y^2+k_z^2\right),\\ H_{XY}&=k_xN_+'k_y+k_yN_-k_x,\end{aligned} \tag{4}$$

where E_v is the valence band edge. Other components are obtained through cyclic permutations of x, y, and z.

The coefficients L', M, N_+', and N_- are derived from the modified Luttinger parameters γ_1, γ_2, and γ_3. Explicitly, these are defined as

$$\begin{aligned}L'&=-\frac{\hbar^2}{2m}\left(\gamma_1+4\gamma_2\right),\\ M&=-\frac{\hbar^2}{2m}\left(\gamma_1-2\gamma_2\right),\\ N'&=-\frac{\hbar^2}{2m}\left(6\gamma_3\right),\\ N_-&=M-\frac{\hbar^2}{2m},\\ N_+'&=-N'-N_-.\end{aligned} \tag{5}$$

The modified Luttinger parameters themselves account for remote band interactions and are expressed as

$$\begin{aligned}\gamma_1&=\gamma_1^L-\frac{E_P}{3E_g},\\ \gamma_2&=\gamma_2^L-\frac{E_P}{6E_g},\\ \gamma_3&=\gamma_3^L-\frac{E_P}{3E_g},\end{aligned} \tag{6}$$

where

$$E_P = \frac{3m/m_c}{\frac{2}{E_g} + 1/(E_g + \Delta)} \tag{7}$$

and γ_1^L, γ_2^L, and γ_3^L are original Luttinger parameters. These parameters refine the representation of heavy-hole and light-hole masses and include effects from higher-energy bands.

Spin-orbit coupling is represented by H_{SO}, a matrix term that introduces band splitting due to the interaction between electron spin and crystal field potential. It is given by:

$$H_{SO} = -\frac{\Delta}{3}\begin{bmatrix} 0 & 0 & 0 & 0 & 0 & 0 & 0 & 0 \\ 0 & 0 & i & 0 & 0 & 0 & 0 & -1 \\ 0 & -i & 0 & 0 & 0 & 0 & 0 & i \\ 0 & 0 & 0 & 0 & 0 & 1 & -i & 0 \\ 0 & 0 & 0 & 0 & 0 & 0 & 0 & 0 \\ 0 & 0 & 0 & 1 & 0 & 0 & -i & 0 \\ 0 & 0 & 0 & i & 0 & i & 0 & 0 \\ 0 & 1 & -i & 0 & 0 & 0 & 0 & 0 \end{bmatrix}. \tag{8}$$

Strain-induced effects are incorporated through H_ε, which modifies the band-structure by accounting for lattice deformation. It can be expressed as [12]:

$$H_\epsilon = \begin{bmatrix} H_{\epsilon 0} & 0 \\ 0 & H_{\epsilon 0} \end{bmatrix} \tag{9}$$

where $H_{\epsilon 0}$ is a 4×4 block given by:

$$H_{\epsilon 0} = \begin{bmatrix} a_c\epsilon & 0 & 0 & 0 \\ 0 & h_{xx} & n\epsilon_{xy} & n\epsilon_{xz} \\ 0 & n\epsilon_{yx} & h_{yy} & n\epsilon_{yz} \\ 0 & n\epsilon_{zx} & n\epsilon_{zy} & h_{zz} \end{bmatrix}. \tag{10}$$

In this matrix, ϵ_{ij} represents the strain tensor components, $\epsilon = \epsilon_{xx} + \epsilon_{yy} + \epsilon_{zz}$, and a_c is the conduction band deformation potential. The diagonal terms, h_{xx}, h_{yy}, and h_{zz}, are defined as:

$$\begin{aligned} h_{xx} &= l\epsilon_{xx} + m\left(\epsilon_{yy} + \epsilon_{zz}\right), \\ h_{yy} &= l\epsilon_{yy} + m\left(\epsilon_{xx} + \epsilon_{zz}\right), \\ h_{zz} &= l\epsilon_{zz} + m\left(\epsilon_{xx} + \epsilon_{yy}\right), \end{aligned} \tag{11}$$

where l, m, and n are parameters expressed in terms of the valence band deformation potentials a_v, b, and d as [12]:

$$\begin{aligned} l &= a_v + 2b, \\ m &= a_v - b, \\ n &= \sqrt{3}\, d. \end{aligned} \tag{12}$$

The strain tensor components are given by [13]:

$$\begin{aligned} \epsilon_{xx} &= \epsilon_{yy} = \frac{a_0 - a}{a}, \\ \epsilon_{zz} &= -\frac{2C_{12}}{C_{11}}\epsilon_{xx}, \\ \epsilon_{xy} &= \epsilon_{yx} = \epsilon_{xz} = \epsilon_{zx} = \epsilon_{yz} = \epsilon_{zy} = 0. \end{aligned} \tag{13}$$

Here, a_0 and a represent the lattice constants of the substrate and the layer material, respectively, while C_{11} and C_{12} are the stiffness constants [14].

After composing Hamiltonian matrix, one needs to find eigenvalues. To address the issue of spurious unphysical solutions, A_c is set to zero [10], simplifying the calculations for the envelope functions ψ_i. The system is governed by the eigenvalue equation:

$$\sum_{j=1}^{9} H_{ij}\psi_j = E\psi_i, \quad i = 1, 2, \cdots, 8 \tag{14}$$

where E is the energy eigenvalue. The scattering matrix method [15] is used to solve this equation. This method is particularly effective for determining the subband dispersions and wave functions in multilayer structures with thick layers. Unlike the transfer-matrix method, which is prone to numerical instability due to the equal treatment of exponentially growing and decaying wave functions, the scattering matrix allows the physically significant eigenstates to dominate. This prevents the loss of decaying wave functions during computation and avoids the need for truncation schemes, making it especially effective for accurately analyzing complex band structures in multilayer systems.

The conduction band envelope functions ψ_1 and ψ_5 are expressed in terms of valence band envelope functions as:

$$\begin{aligned} \psi_1 &= i\left(E - E_c - a_c\epsilon\right)^{-1} P(k_x\psi_2 + k_y\psi_3 + k_z\psi_4), \\ \psi_5 &= i\left(E - E_c - a_c\epsilon\right)^{-1} P(k_x\psi_6 + k_y\psi_7 + k_z\psi_8). \end{aligned} \tag{15}$$

Substituting these expressions into the remaining six equations reduces the system to a 6×6 energy-dependent Hamiltonian $H^{(e)}$ governing the evolution of the vector $\mathbf{F} = \left[\psi_2\psi_3\psi_4\psi_6\psi_7\psi_8\right]^T$:

$$H^{(e)}\mathbf{F} = E\mathbf{F}. \tag{16}$$

The matrix $H^{(e)}$ is obtained by removing the conduction band rows and columns from H and updating the parameters L and N_+ as follows:

$$\begin{aligned} L(E) &= L' + \frac{P^2}{E - E_c - a_c\epsilon}, \\ N_+(E) &= N_+' + \frac{P^2}{E - E_c - a_c\epsilon}. \end{aligned} \tag{17}$$

Eq. (16) should be solved in each layer of the structure using plane waves. The wavefunctions are then matched at the interfaces by applying the boundary conditions from Burt's envelope function theory [16], which are derived by integrating Eq. (16) across the interfaces. As a result, the vector functions $\mathbf{F}$ and $B\mathbf{F}$ must be continuous. The 6×6 matrix B is given by:

$$B = \begin{bmatrix} B_3 & 0 \\ 0 & B_3 \end{bmatrix} \tag{18}$$

where the 3×3 block B_3 is defined as:

$$B_3 = \begin{bmatrix} M\,\partial/\partial z & 0 & iN\_k_x \\ 0 & M\,\partial/\partial z & iN\_k_y \\ iN_+k_x & iN_+k_y & L\,\partial/\partial z \end{bmatrix}. \tag{19}$$

The solution of $H^{(e)}$in each quantum well layer n is expressed as a superposition of transmitted and reflected plane waves with the same energy E and in-plane vector (k_x, k_y):

$$\mathbf{F} = e^{i(k_x x + k_y y)} \sum_{j=1}^{6} \left\{ a_j^{(n)} e^{ik_{zj}^{(n)}(z - z_{n1})} \mathbf{e}_{+j}^{(n)} + b_j^{(n)} e^{-ik_{zj}^{(n)}(z - z_{n2})} \mathbf{e}_{-j}^{(n)} \right\}. \quad (20)$$

Here, $k_{z,j}^{(n)}(j = 1, \cdots, 6)$ are the z-components of the complex wave vectors for the bulk states, with positive or zero imaginary parts. The coefficients $a_j^{(n)}$ and $b_j^{(n)}$ represent the transmitted and reflected wave amplitudes, respectively, and $\mathbf{e}_{\pm j}^{(n)}$ are the eigenvectors satisfying:

$$H^{(e)}\left(\pm k_{z,j}\right)\mathbf{e}_{\pm j}^{(n)} = E\mathbf{e}_{\pm j}^{(n)} \quad (21)$$

where $H^{(e)}\left(\pm k_{z,j}\right)$ matrices are derived from the matrix $H^{(e)}$ by substituting k_z with $\pm k_{z,j}$ where $k_{z,j}$ satisfy the equation $\left|H^{(e)}\left(k_{z,j}\right) - EI\right| = 0$, with I representing the identity matrix.

Under the given boundary conditions, the coefficients of two neighboring layers are connected using the transfer matrix. The relationship is expressed as:

$$M^{(n+1)} = \begin{bmatrix} D^{(n)^{-1}} & 0 \\ 0 & I \end{bmatrix} \bar{M}^{(n+1)} \begin{bmatrix} I & 0 \\ 0 & D^{(n+1)} \end{bmatrix} \quad (22)$$

where I is the 3×3 identity matrix, and $D^{(n)}$ is a 3×3 diagonal matrix with elements:

$$D_{ij}^{(n)} = \delta_{ij} e^{ik_{zj}^{(n)}(y_n - y_{n-1})}. \quad (23)$$

Since $D^{(n)}$ is diagonal, its inverse is obtained by inverting each diagonal element. The matrix $\bar{M}^{(n+1)}$ is nonsingular and invertible, given by:

$$\bar{M}^{(n+1)} = \begin{bmatrix} \mathbf{e}_+^{(n)} & \mathbf{e}_-^{(n)} \\ \mathbf{f}_+^{(n)} & \mathbf{f}_-^{(n)} \end{bmatrix}^{-1} \begin{bmatrix} \mathbf{e}_+^{(n+1)} & \mathbf{e}_-^{(n+1)} \\ \mathbf{f}_+^{(n+1)} & \mathbf{f}_-^{(n+1)} \end{bmatrix} \quad (24)$$

where $\mathbf{e}_\pm^{(n)} = \left[\mathbf{e}_{\pm 1}^{(n)}\, \mathbf{e}_{\pm 2}^{(n)}\, \mathbf{e}_{\pm 3}^{(n)}\right]$ and $\mathbf{f}_\pm^{(n)} = \left[\mathbf{f}_{\pm 1}^{(n)}\, \mathbf{f}_{\pm 2}^{(n)}\, \mathbf{f}_{\pm 3}^{(n)}\right]$. Additionally:

$$\mathbf{f}_{\pm j}^{(n)} = B\mathbf{e}_{\pm j}^{(n)}. \quad (25)$$

The coefficients of outgoing waves $\left(a^{(n)},\ b^{(m)}\right)$ and incoming waves $\left(a^{(m)},\ b^{(n)}\right)$ are related through the scattering matrix $S(m.\ n)$:

$$\begin{bmatrix} a^{(n)} \\ b^{(m)} \end{bmatrix} = S(m,n) \begin{bmatrix} a^{(m)} \\ b^{(n)} \end{bmatrix}. \quad (26)$$

Using the transfer matrix equation, a recursive formula for the submatrices of $S(m, n)$ is derived:

$$S_{11}(1,n+1) = \left[I - M_{11}^{(n+1)^{-1}} S_{12}(1,n) M_{21}^{(n+1)}\right]^{-1} M_{11}^{(n+1)^{-1}} S_{11}, \quad (27)$$

$$S_{12}(1,n+1) = \left[I - M_{11}^{(n+1)^{-1}} S_{12}(1,n) M_{21}^{(n+1)}\right]^{-1} M_{11}^{(n+1)^{-1}} \left[S_{12}(1,n) M_{22}^{(n+1)} - M_{12}^{(n+1)}\right],$$

$$S_{21}(1,n+1) = S_{22}(1,n) M_{21}^{(n+1)} S_{11}(1,n+1) + S_{21}(1,n),$$

$$S_{22}(1,n+1) = S_{22}(1,n) M_{21}^{(n+1)} S_{12}(1,n+1) + S_{22}(1,n) M_{22}^{(n+1)}.$$

The submatrices of $M^{(n+1)}$ are obtained as:

$$M_{11}^{(n+1)} = \left[\bar{M}_{11}^{(n+1)^{-1}} D^{(n)}\right]^{-1}, \quad (28)$$

$$M_{12}^{(n+1)} = D^{(n)^{-1}} \bar{M}_{12}^{(n+1)} D^{(n+1)},$$

$$M_{21}^{(n+1)} = \bar{M}_{21}^{(n+1)},$$

$$M_{22}^{(n+1)} = \bar{M}_{22}^{(n+1)} D^{(n+1)}.$$

By setting $S(1, 1) = I$, the recursive relations allow constructing all scattering matrices $S(1, n)$ for $n = 2, 3, \cdots, N$. Similarly, setting $S(m, m) = I$, all $S(m, n)$ for $n > m$ can be constructed.

The coefficients of incoming waves $a^{(1)}$ and $b^{(N)}$ are set to zero to determine the energy levels of states confined in the quantum well. Using:

$$M_{11}^{(n+1)} = \left[\bar{M}_{11}^{(n+1)^{-1}} D^{(n)}\right]^{-1}, \quad (29)$$

$$M_{12}^{(n+1)} = D^{(n)^{-1}} \bar{M}_{12}^{(n+1)} D^{(n+1)},$$

$$M_{21}^{(n+1)} = \bar{M}_{21}^{(n+1)},$$

$$M_{22}^{(n+1)} = \bar{M}_{22}^{(n+1)} D^{(n+1)}.$$

To determine the coefficients for n^{th} layer of an N-layer structure, we have:

$$\begin{bmatrix} a^{(n)} \\ b^{(1)} \end{bmatrix} = S(1,n) \begin{bmatrix} a^{(1)} \\ b^{(n)} \end{bmatrix}, \quad (30)$$

$$\begin{bmatrix} a^{(N)} \\ b^{(n)} \end{bmatrix} = S(n,N) \begin{bmatrix} a^{(n)} \\ b^{(N)} \end{bmatrix}.$$

The coefficients of incoming waves $a^{(1)}$ and $b^{(N)}$ are set to zero to determine the energy levels of states confined in the superlattice period. From these, the coefficients $a^{(n)}$ and $b^{(n)}$ are determined as:

$$a^{(n)} = \left[I - S_{12}(1,n) S_{21}(n,N)\right]^{-1} \times \left[S_{11}(1,n) a^{(1)} + S_{12}(1,n) S_{22}(n,N) b^{(N)}\right], \quad (31)$$

$$b^{(n)} = \left[I - S_{21}(n,N) S_{12}(1,n)\right]^{-1} \times \left[S_{21}(n,N) S_{11}(1,n) a^{(1)} + S_{22}(n,N) b^{(N)}\right].$$

To describe the superlattice electronic structure and determine energy levels, periodic boundary conditions must be introduced. For a superlattice, the coefficients of each layer within a period must match the coefficients of the corresponding layer in the next period. For example:

$$\begin{bmatrix} a^{(N)} \\ b^{(1)} \end{bmatrix} = S(1,N) \begin{bmatrix} a^{(1)} \\ b^{(N)} \end{bmatrix}, \quad (32)$$

$$\begin{bmatrix} a^{(1)} \\ b^{(1)} \end{bmatrix} = \begin{bmatrix} a^{(N)} \\ b^{(N)} \end{bmatrix}.$$

As a result, the following equation must be solved to find the energy levels:

$$\left[S(1,N) - I\right] \begin{bmatrix} a^{(N)} \\ b^{(1)} \end{bmatrix} = 0, \quad (33)$$

or equivalently:

$$\left|S(1,N) - I\right| = 0, \quad (1)$$

Once the energy levels of the system are determined, the coefficients $a^{(n)}$ and $b^{(n)}$ for each layer can be calculated using the expressions derived above.

2 Comparison with experimental results

Using the discussed scattering matrix-based method, we calculated the electronic band-structure of LWIR

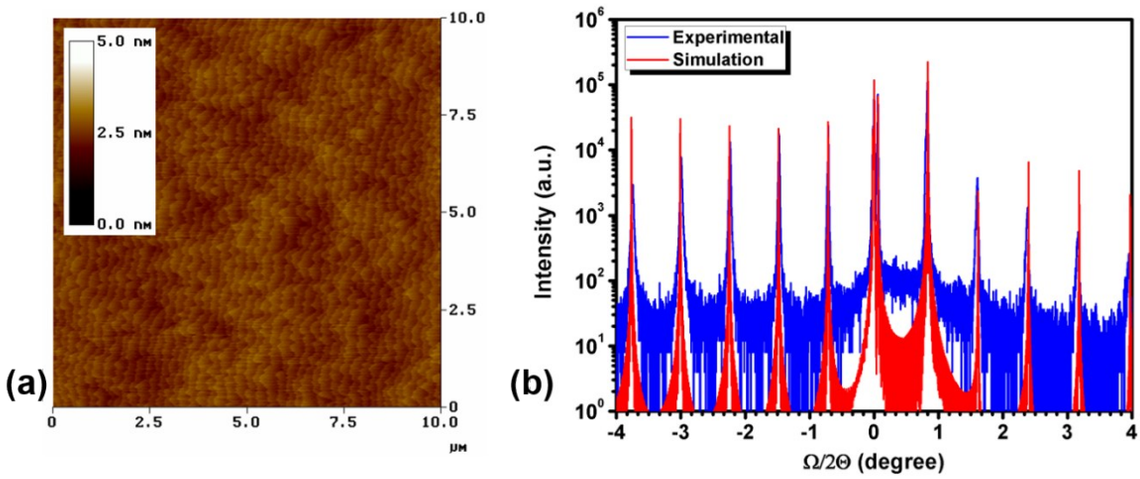

Fig. 1 (a) The atomic force microscopy image of a 10 × 10 μm^2 surface area of one of the LWIR samples used in this study with rms roughness value of 1.3 Å. (b) High-resolution X-ray diffraction (HR-XRD) rocking curve and simulation for the same device.

InAs/GaSb superlattices. The accuracy of the method was validated by comparing calculated cutoff wavelengths to experimental data, demonstrating the precision of this approach.

The samples for this work were grown on *n*-type GaSb substrates using a solid source molecular beam epitaxy (SSMBE) reactor equipped with group III SUMO® cells and group V valved crackers. The quality of the material was assessed after epitaxial growth using atomic force microscopy (AFM) and high-resolution X-ray diffraction (HR-XRD). The samples exhibited good surface morphology, characterized by clear atomic steps and a small surface roughness of less than 1.5 Å over a 10 × 10 μm^2 area, indicating the absence of structural degradation. The satellite peaks in the HR-XRD scan showed the overall periods of the superlattices. The lattice mismatch to the GaSb substrate for all samples was less than 2000 ppm (Figure 1). In Figure 2, we present examples of the photoluminescence (PL) and quantum efficiency (QE) spectra of a photodiode fabricated from one of the LWIR superlattices used in this study at 77 K. The superlattice design consists of 13 and 7 monolayers (MLs) of InAs and GaSb, respectively, with InSb-like interface layers.

The superlattice layer thicknesses for each sample were extracted from HR-XRD results using a method described in Ref. [17] and fed into model to make the electronic band-structure estimation as accurate as possible. The deviations between calculated and measured wavelengths, $\Delta\lambda = \lambda_{cutoff} - \lambda_{calc}$, are plotted in Figure 3. All samples exhibited deviations within 0.4 μm, with the majority falling below 0.2 μm, highlighting the reliability of this approach.

The thermal effects were also considered, as indicated by red and green lines in Figure 3, which represent the error margin arising from a variation of $\pm k_B T$ in the bandgap energy at 77 K. Since InAs/GaSb superlattices are often employed as absorbers in infrared detectors operating at 77 K, it is significant that all points lie within these bonds. This alignment underscores that wavelength

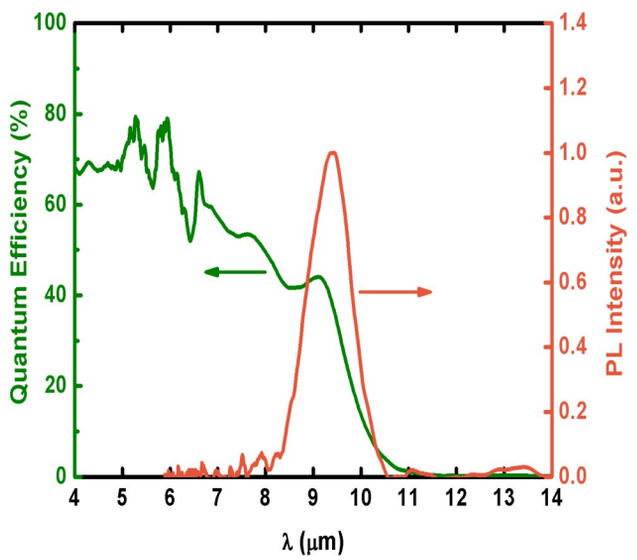

Fig. 2 Quantum efficiency and normalized PL spectra at 77K for one of the LWIR samples used in this study.

deviations are predominantly below typical thermal broadening, further demonstrating the precision of our method.

3 Conclusions

We have investigated the electronic band-structure modeling of InAs/GaSb type-II superlattices using a scattering matrix-based approach that incorporates boundary condition matching and interface dynamics. The model's theoretical predictions show strong agreement with experimental results, demonstrating its accuracy in capturing the electronic properties of InAs/GaSb superlattices. These results support the method's effectiveness in providing a detailed understanding of the band structure and its potential utility in the analysis and design of superlattice structures.

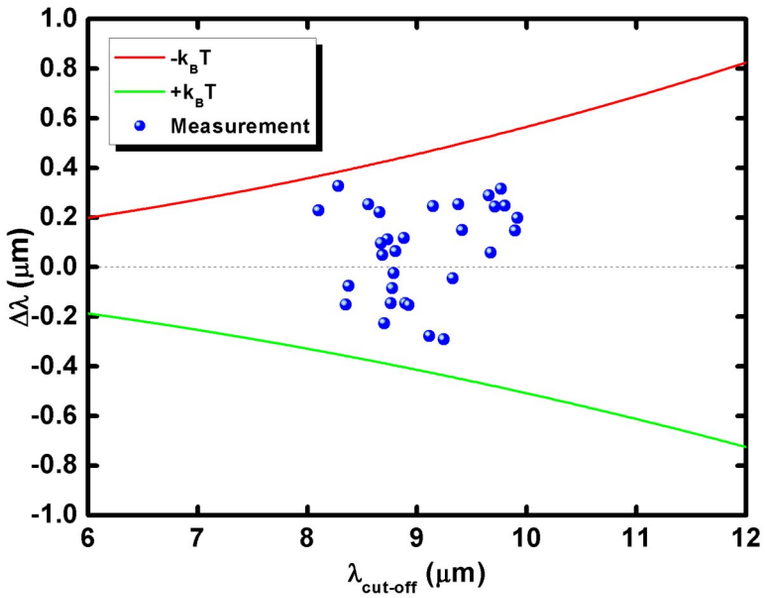

Fig. 3 Deviation of predicted cutoff wavelengths from the measured cutoff wavelengths. The red and green lines indicate the effect of an error of k_BT in band-gap energy at 77 K.

References

[1] SAI-HALASZ G A, TSU R, ESAKI L. A new semiconductor superlattice[J]. Applied Physics Letters, 1977, 30(12): 651-653.

[2] POUR S A, HUANG E K, CHEN G, et al. High operating temperature midwave infrared photodiodes and focal plane arrays based on type-II InAs/GaSb superlattices[J]. Applied Physics Letters, 2011, 98(14): 143501.

[3] NGUYEN B M, HOFFMAN D, HUANG E K W, et al. Background limited long wavelength infrared type-II InAs/GaSb superlattice photodiodes operating at 110 K[J]. Applied Physics Letters, 2008, 93(12): 123502.

[4] YANG R Q, YANG B H, ZHANG D, et al. High power mid-infrared interband cascade lasers based on type-II quantum wells[J]. Applied Physics Letters, 1997, 71(17): 2409-2411.

[5] WEI Y, GIN A, RAZEGHI M, et al. Advanced InAs/GaSb superlattice photovoltaic detectors for very long wavelength infrared applications[J]. Applied Physics Letters, 2002, 80(18): 3262-3264.

[6] NGUYEN B M, HOFFMAN D, DELAUNAY P Y, et al. Dark current suppression in type II InAs/GaSb superlattice long wavelength infrared photodiodes with M-structure barrier[J]. Applied Physics Letters, 2007, 91(16): 163511.

[7] NGUYEN B M, BOGDANOV S, POUR S A, et al. Minority electron unipolar photodetectors based on type II InAs/GaSb/AlSb superlattices for very long wavelength infrared detection[J]. Applied Physics Letters, 2009, 95(18): 183502.

[8] WEI Y, RAZEGHI M. Modeling of type-II InAs/GaSb superlattices using an empirical tight-binding method and interface engineering [J]. Physical Review B, 2004, 69(8): 085316.

[9] BURT M G. The justification for applying the effective-mass approximation to microstructures[J]. Journal of Physics: Condensed Matter, 1992, 4(32): 6651-6690.

[10] FOREMAN B A. Elimination of spurious solutions from eight-band k·p theory [J]. Physical Review B, 1997, 56(20): R12748-R12751.

[11] GALERIU C. kp Theory of Semiconductor Nanostructures [D]. Worcester: Worcester Polytechnic Institute, 2005.

[12] BIR G L, PIKUS G E. Symmetry and strain-induced effects in semiconductors[M]. New York: Wiley, 1974.

[13] CHAO C Y P, CHUANG S L. Spin-orbit-coupling effects on the valence-band structure of strained semiconductor quantum wells [J]. Physical Review B, 1992, 46(7): 4110-4122.

[14] VAN DE WALLE C G. Band lineups and deformation potentials in the model-solid theory[J]. Physical Review B, 1989, 39(3): 1871-1883.

[15] KO D Y K, INKSON J C. Matrix method for tunneling in heterostructures: Resonant tunneling in multilayer systems[J]. Physical Review B, 1988, 38(14): 9945-9951.

[16] BURT M G. The justification for applying the effective-mass approximation to microstructures[J]. Journal of Physics: Condensed Matter, 1992, 4(32): 6651-6690.

[17] LIVNEH Y, KLIPSTEIN P C, KLIN O, et al. Model for the energy dispersions and absorption spectra of InAs/GaSb type-II superlattices [J]. Physical Review B, 2012, 86(23): 235311.